International Journal of GEOMATE, May, 2024 Vol.26, Issue 117, pp.68-77
ISSN: 2186-2982 (P), 2186-2990 (O), Japan, DOI: https://doi.org/10.21660/2024.117.g13174
Geotechnique, Construction Materials and Environment

A NEW TYPE OF ELECTROMAGNETIC VIBRATION ACTUATOR CAPABLE OF COMBINED LINEAR AND ROTATIONAL MOTIONS

* Hiroyuki Yaguchi[1] and Ryusei Sato[1]

[1]Faculty of Engineering, Tohoku Gakuin University, Japan

*Corresponding Author, Received: 01 June 2023, Revised: 26 Feb. 2024, Accepted: 27 Feb. 2024

ABSTRACT: The deterioration of large steel structures, such as bridges and power generation facilities built in the 1960s, has become a problem. Such infrastructure requires regular inspections every few years, and many robots have been proposed for structural inspection. However, inspection technology for large steel structures by robots has not yet been established. The establishment of inspection technology in bridges is one of the most important issues in the maintenance of social infrastructure. This paper proposes a novel vibration actuator as a new robot drive source, which combines mechanical resonance and electromagnetic force and enables reciprocating movement by orthogonally arranging multiple vibration components. By controlling the phase difference of these vibration components with only a simple signal generator and amplifier, machine tests showed that reciprocating and rotating reciprocating motions with almost the same characteristics are possible. Experimental results reveal that the vibration actuator is able to pull a load mass of 150 g. In addition, motion analysis is conducted by applying the energy method and considering the effects of phase control on the linear and rotational motions of the vibration actuator. The results obtained in the machine test and the analysis results are mostly in agreement. This confirms that even if the parameters for the vibration actuator are varied, the linear and rotational characteristics of the actuator can be predicted by theoretical calculations. A new drive source for robots and the operation of electromagnetic motors capable of linear and rotational motion are established in this paper. For this reason, the possibility of realizing social infrastructure improvement for large steel structures such as bridges is demonstrated.

Keywords: Vibration, Actuator, Phase control, Linear and rotational motions, Motion analysis

1. INTRODUCTION

The deterioration of large steel structures such as bridges and power generation facilities built in the 1960s has become a problem. In particular, there is concern about the safety of bridges constructed more than 50 years ago. Cracks have been reported in some bridges due to the increased traffic volume of large vehicles. Since these old social infrastructures were built without seismic standards, accidents involving falling bridges due to aging have been frequent in natural disasters. To prevent such accidents, efficient and regular inspections of aging bridges are necessary.

To solve these problems, many inspection robots, such as electromagnetic [1], roller [2-4], and magnetic-wheel type [5-9] robots, have been proposed to improve worker safety and reduce costs. However, these robots use an electromagnetic motor as the drive source. Reduction gears and additional devices between the motor and the driving mechanism are thus required. Moreover, these robots need to be equipped with many electromagnetic motors to move along a structure. This increases weight and limits movement characteristics. Many flying robots, such as drones [10-13], have also been proposed.

However, these robots are difficult to operate and are easily affected by rain and wind. Thus, despite the development of numerous robots and actuators, the technology for inspecting structures has not yet been fully established. Therefore, a new actuator that is lightweight, controllable, and capable of direct drive is needed. Although methods based on theoretical analysis [14-16] have been attempted, the establishment of inspection technology for bridges using robots is one of the most important issues in the maintenance and management of social infrastructure.

Usually, vibration phenomena are considered harmful and controlled [17-19]. On the other hand, the authors proposed a new actuator for a robot drive source by combining mechanical resonance and electromagnetic force. These actuators consist of multiple vibration components arranged orthogonally and are capable of reciprocating motion by controlling the phase difference of the vibrations [20-21]. Further, these actuators can be driven directly; they are smaller, lighter, and more controllable than existing robots.

However, this actuator can only perform linear motion (i.e., it cannot be rotated), which greatly limits its possible movement directions. A vibration actuator capable of instantaneous linear and rotary reciprocating movement is newly proposed in this paper. The vibration actuator with three orthogonally arranged vibration components is proposed in this study. Machine tests show that by controlling

the phase difference among these components, reciprocating and rotational reciprocating movements with almost the same characteristics are possible. Furthermore, the energy method proposed by the authors [20] was applied, a new static analysis method was proposed for linear and rotational motions of actuators in which the phase difference of vibration was taken into account. The experimental and calculated results are found to agree relatively well, verifying the validity of the theoretical analysis. The proposed vibration actuator can move in a 360-degree range by rotating, allowing it to perform the same motion as that of a robot equipped with multiple motors. Design criteria for the actuator based on static analysis were also established in this study. This actuator has excellent propulsion characteristics and can be equipped with a CCD camera. The possibility of realizing social infrastructure improvement for large steel structures such as bridges is demonstrated.

A future task is to theoretically calculate the vibration amplitudes of the vibration components. This requires a vibration analysis that takes into account the nonlinearity of the vibration component. Furthermore, by further improving the magnetic circuit of the vibration components proposed by the authors [22], the propulsive force of the actuator can be increased and applied as a driving source for a robot. This vibration actuator is capable of coordinated operation of linear and rotational motion and can be applied as a new electromagnetic motor in various industrial fields.

As described above, many inspection robots have been developed, but inspection technology has not yet been established. The purpose of this study is to propose a new electromagnetic vibration actuator that can move freely over a 360-degree angle and to clarify its operation through actual machine tests and theoretical static analysis. The results of the actual machine test and the analysis are in good agreement, and the principle of operation of the new vibration actuator, which can be operated by phase control of three vibration components, is established in this paper.

2. RESEARCH SIGNIFICANCE

Fatigue of bridges has become a problem due to increased traffic. Although various types of robots have been developed, inspection techniques have not yet been established. Based on these considerations, a study was conducted to establish operation in a new actuator that is lightweight, compact, and has high movement characteristics, which could be used as a driving source for a robot. The significance of this research is to establish a device for bridge inspection and to provide an answer to social demands.

3. STRUCTURE OF PROPOSED VIBRATION ACTUATOR

Fig. 1 shows a vibration actuator capable of moving a magnetic material in a plane. This actuator consists of three vibration components A, B and C with the same specifications, an acrylic frame, an acrylic plate, three NdFeB magnets and natural rubber attached to the bottom of the acrylic frame. The center permanent magnet (main magnet) was used to hold the actuator to the magnetic material. On the other hand, the other two permanent magnets (secondary magnets) were attached to stabilize the linear motion of the actuator. The secondary magnets are mounted at positions 22 mm from the center of the actuator. The main magnet has a diameter D of 10 mm and a thickness of 2 mm. The secondary permanent magnets have a diameter of d = 6 mm and a thickness of 1 mm. In addition, a natural rubber sheet with a thickness of 1 mm is attached to the lower part of the three permanent magnets to increase the frictional force.

Component A is mounted in the center of the frame, and components B and C are arranged orthogonally and parallel to it, respectively. A vibration component consists of a cylindrical permanent magnet, a translational spring, an electromagnet, and an acrylic plate. The translational spring is made of stainless steel and has an outer diameter of 12 mm, a free length of 25 mm, and a spring constant of k = 1,836 N/m. The Permanent

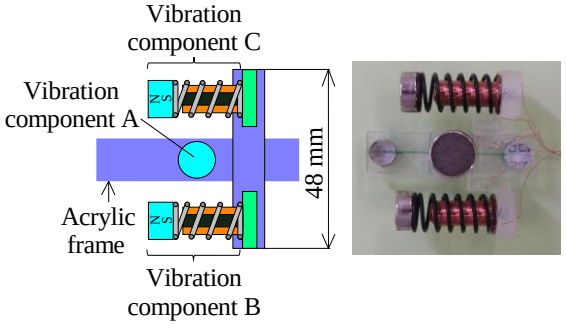

(a) Plan view

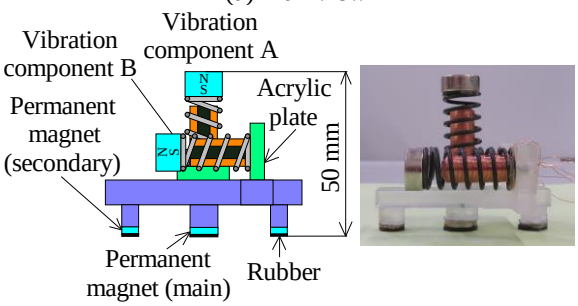

(b) Front view

Fig. 1. Structure of proposed vibration actuator

magnet is a cylindrical NdFeB magnet magnetized in the axial direction. It is 12 mm in diameter and 5 mm in height. The electromagnet consists of an iron core (diameter: 3.75 mm) with 840 turns of copper wire (diameter: 0.2 mm). The electromagnetic excitation force due to attraction and repulsion during one period of vibration acts on the permanent magnet. The vibration actuator has a height of 50 mm, a length of 52 mm, a width of 48 mm, and a total mass M_a of 53 g.

4. PRINCIPLE OF OPERATION FOR PROPOSED VIBRATION ACTUATOR

As shown in Fig. 2, the proposed vibration actuator has two vibration components (B and C) arranged orthogonally to vibration component A. By controlling the phase difference among components A, B and C, reciprocating movement with linear and rotational motions is possible. It is assumed that the vibration amplitudes of components B and C are equal. For components A, B, and C, displacement coordinates y and x are defined as shown in Fig. 2. The attractive force exerted by the main magnet attached to the frame is P_1 and that exerted by the secondary magnets is P_2. As shown in Fig. 2, the vibration amplitude and the force generated during

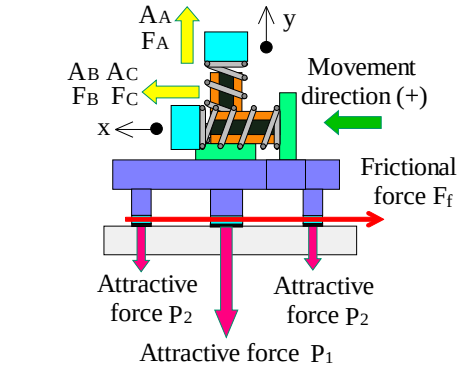

(a) Sliding

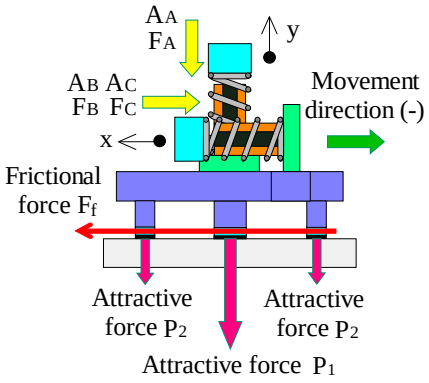

(b) Small amount of sliding

Fig. 2. Principle of linear motion

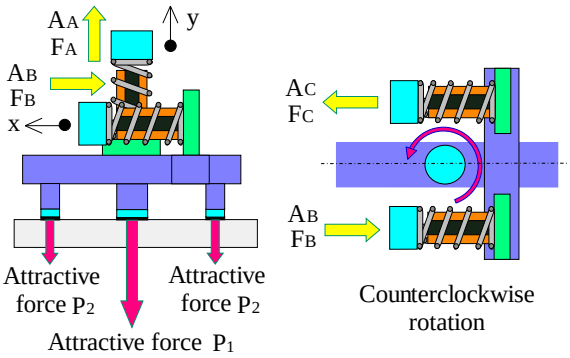

(a) Rotation

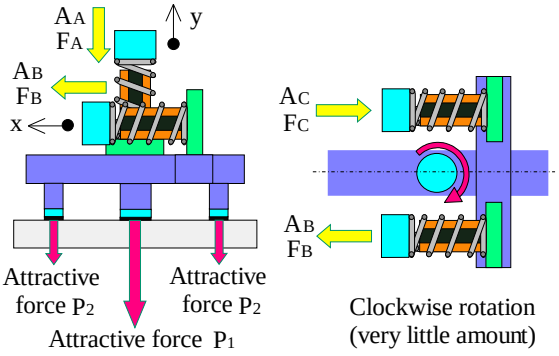

(b) Small amount of rotation

Fig. 3. Principle of rotational motion

vibration for components A, B, and C are denoted as A_A, A_B, A_C and F_A, F_B, F_C, respectively.

We now consider linear motion when components A, B, and C are resonantly driven at an angular frequency ω. One period of oscillation ($\omega/2\pi$) is considered. As shown in Fig. 2(a), when component A is displaced in the +y direction with an amplitude A_A, the force F_A is generated by the component reduces the frictional force E_f. In this state, when components B and C are displaced in the +x direction with amplitudes A_B and A_C, respectively, the generated forces F_B and F_C cause the actuator to slip in the +x direction. This state is defined as forward displacement.

On the other hand, as shown in Fig. 2(b), when the permanent magnet of vibration component A is displaced in the -y direction with an amplitude A_A, the force F_A generated increases the frictional force F_f. Therefore, even if components B and C are displaced in the -x direction with amplitudes A_B and A_C to generate forces F_B and F_C, respectively, the movement of the actuator in the -x direction is small. This state is defined as backward displacement.

In this manner, the frictional force E_f for the permanent magnet at the holding part of the actuator is periodically changed, allowing the actuator to move in the +x direction by repeating forward and backward motions. By setting the phase difference among the vibrations for components A, B, and C to

180 degrees (i.e., antiphase), the actuator can move in the -x direction.

The motion principle described above can also be extended to rotational motion. As shown in Fig. 3(a), when component A is displaced in the +y direction with an amplitude A_A, the frictional force E_f is reduced by the generated force F_A, as in the case of linear movement. When component B is displaced with an amplitude A_B in the -x direction and component C is displaced with an amplitude A_C in the +x direction, a moment acts on the frame center due to forces F_B and F_C. The vibration actuator can thus rotate counterclockwise, as shown in Fig. 3(a).

On the other hand, as shown in Fig. 3(b), when component A is displaced in the -y direction with an amplitude of A, component B is displaced in the +x direction with an amplitude A_B and component C is displaced in the -x direction with an amplitude of A_C. However, due to the increase in frictional force F_f, it is difficult for the actuator to rotate clockwise.

According to the operating principle described above, the actuator can be rotated clockwise or counterclockwise by controlling the phase difference among the vibrations of the three components.

5. MOTION ANALYSIS OF VIBRATION ACTUATOR USING ENERGY METHOD

5.1 Linear Motion

To establish the principle of operation, a static analysis was performed on the linear movement of the actuator. The linear motion of this actuator will be analyzed using the energy method [15]. As shown in Fig. 4 (a) and (b), let us consider the state in which the actuator is attached to a magnetic material with a slope angle β by the attractive force of the permanent magnets. As mentioned above, the permanent magnets of components B and C are considered to vibrate with the same phase in the case of linear motion. We also assume that the vibration amplitudes of components B and C are equal. Let k be the spring constant for the vibration components, m be the total mass of the actuator, and M be the load mass. The coefficient of friction between the rubber sheet and the slope is μ. With g as the gravitational acceleration, the frictional force F_f when the actuator is climbing up the slope is as follows.

$$F_f = \mu\{(m+M)\, g\cos\beta + P_1 + 2P_2 - F_A\} \quad (1)$$

The balance of forces along the slope yields

$$F_B + F_C = F_f + (m+M)\, g\sin\beta \quad (2)$$

On the other hand, when the actuator is going down the slope, the friction force F_b is as follows.

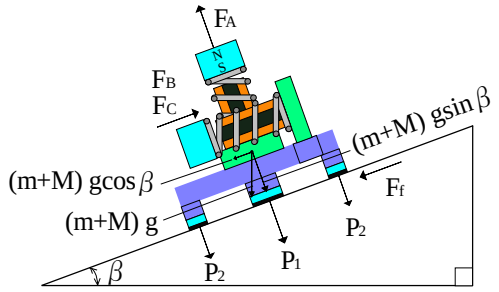

(a) Balance of forward movement

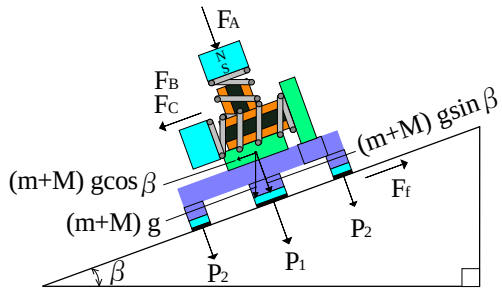

(b) Balance of backward movement

Fig. 4. Actuator moving on slope with angle β

$$F_b = \mu\{(m+M)\, g\cos\beta + P_1 + 2P_2 + F_A\} \quad (3)$$

The balance of forces along the slope yields

$$F_B + F_C = F_b - (m+M)\, g\sin\beta \quad (4)$$

The elastic energy U generated by components B and C is set equal to the dissipated energy $F_f \times \delta_f$, $F_b \times \delta_b$ due to the frictional force and the work done by gravity. Since the vibration amplitudes of components B and C are equal, the following equation is obtained:

$$\left.\begin{aligned} 2U = [\,&\mu\{(m+M)\, g\cos\beta + P_1 + 2P_2 - F_A\} \\ &+ (m+M)\, g\sin\beta\,]\,\delta_f \\ 2U = [\,&\mu\{(m+M)\, g\cos\beta + P_1 + 2P_2 + F_A\} \\ &- (m+M)\, g\sin\beta\,]\,\delta_b \end{aligned}\right\} \quad (5)$$

Where

$$U = \frac{1}{2}k A_B^2 = \frac{1}{2}k A_C^2 \quad (6)$$

From equation (5), the forward and backward displacements, δ_f and δ_b, are expressed as follows.

$$\left.\begin{aligned} \delta_f &= \frac{2U}{\mu\{(m+M)g\cos\beta + P_1 + 2P_2 - F_A\} + (m+M)\, g\sin\beta} \\ \delta_b &= \frac{2U}{\mu\{(m+M)g\cos\beta + P_1 + 2P_2 + F_A\} - (m+M)\, g\sin\beta} \end{aligned}\right\} \quad \cdots\cdots(7)$$

As $F_A = k \times A_A$ in the above equations, the following dimensionless quantities and quantities are introduced.

$$\left.\begin{array}{c} \overline{F}_A = F_A/P_1, \quad \overline{P}_2 = P_2/P_1, \quad \overline{m} = mg/P_1 \\ \overline{M} = Mg/P_1, \quad \overline{U} = U/P_1 \end{array}\right\} \quad (8)$$

If the phase difference among vibration components A, B, and C is τ and equation (8) is used, equation (7) can be expressed as follows.

$$\left.\begin{array}{l} \delta_f = \dfrac{2\overline{U}\cos\tau}{\mu\left\{\left(\overline{m}+\overline{M}\right)\cos\beta + 1 + 2\overline{P}_2 - \overline{F}_A\right\} + \left(\overline{m}+\overline{M}\right)\sin\beta} \\ \delta_b = \dfrac{2\overline{U}\cos\tau}{\mu\left\{\left(\overline{m}+\overline{M}\right)\cos\beta + 1 + 2\overline{P}_2 + \overline{F}_A\right\} - \left(\overline{m}+\overline{M}\right)\sin\beta} \end{array}\right\} \quad \cdots\cdots (9)$$

Since the displacement of per one period of vibration is (δ_f - δ_b), if the driving frequency of the vibration component denoted as f (Hz), the linear speed v (mm/s) of the actuator can be obtained as follows.

$$v = f\left(\delta_f - \delta_b\right) \quad (10)$$

5.2 Rotational Motion

A static analysis is now performed on the rotational motion of the vibration actuator. As shown in Fig. 5, the rotational motion of the actuator placed on a plane is investigated. A permanent magnet with attractive force P_2 is attached at r = 22 mm from the center of the actuator. Vibration components B and C are attached at R = 18 mm from the center.

The moment N due to the frictional force when the main magnet rotates around the center with radius D = 10 mm is considered. Under the assumption that W is the total force acting on the main magnet, the moment N is expressed as follows from the thrust bearing analysis results [23].

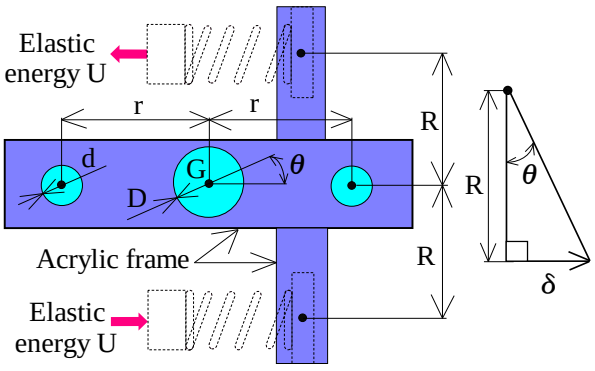

Fig. 5. Actuator specifications for rotational motion

$$N = \frac{2}{3}\mu W D \ , \quad W = mg + P_1 \quad (11)$$

in the +y direction with an amplitude A_A and generates a force F_A, the moment N_f due to the frictional force around the actuator center G is expressed as follows from the relationship in equation (11).

$$N_f = 2\mu P_2 r + \frac{2}{3}\mu\left(mg + P_1 - F_A\right) D \quad (12)$$

On the other hand, when component A vibrates in the -y direction with an amplitude A_A, the moment N_b due to the frictional force around the center G of the actuator is expressed as follows.

$$N_b = 2\mu P_2 r + \frac{2}{3}\mu\left(mg + P_1 + F_A\right) D \quad (13)$$

In the case of rotational motion, components B and C are considered to vibrate in opposite phases. By setting the elastic energy U generated by components B and C in equation (6) equal to the moment dissipation energies $N_f \times \delta_f$ and $N_b \times \delta_b$ due to frictional forces, the forward and backward angular displacements, δ_f and δ_b, are expressed as follows.

$$\left.\begin{array}{l} \delta_f = \dfrac{2UR}{2\mu P_2 r + \frac{2}{3}\mu\left(mg + P_1 - F_A\right) D} \\ \delta_b = \dfrac{2UR}{2\mu P_2 r + \frac{2}{3}\mu\left(mg + P_1 + F_A\right) D} \end{array}\right\} \quad (14)$$

Equation (14) shows the case where the total force and force F_A generated by component A act only on the main magnet. On the other hand, the forces acting on the main and secondary magnets with areas S_1 and S_2, respectively, are distributed based on the area. Equation (8) and the following dimensionless quantities are introduced into equation (14).

$$\bar{r} = r/R \ , \quad \overline{D} = D/R \quad (15)$$

If the phase difference among A, B, and C is τ, assuming that the total area of the permanent magnet is S (=S_1+2S_2), the following relationship is obtained for the forward and backward angular displacements.

$$\delta_f = \frac{2\overline{U}\cos\tau}{2\mu\xi_1\bar{r} + \frac{2}{3}\mu\xi_2\overline{D}} \quad , \quad \delta_b = \frac{2\overline{U}\cos\tau}{2\mu\xi_3\bar{r} + \frac{2}{3}\mu\xi_4\overline{D}} \quad \cdots\cdots (16)$$

Where

$$\left.\begin{aligned}\xi_1 &= \overline{P}_2 + (S_2/S)\overline{m} - (S_2/S)\overline{F}_A \\ \xi_2 &= (S_1/S)\overline{m} + 1 - (S_1/S)\overline{F}_A \\ \xi_3 &= \overline{P}_2 + (S_2/S)\overline{m} + (S_2/S)\overline{F}_A \\ \xi_4 &= (S_1/S)\overline{m} + 1 + (S_1/S)\overline{F}_A\end{aligned}\right\} \quad (17)$$

The displacement δ per one cycle of vibration is as follows.

$$\delta = \delta_f - \delta_b \quad (18)$$

Referring to Fig. 5, assume the actuator rotates counterclockwise. Then, the rotation angle θ during one period of vibration is expressed as follows.

$$\tan\theta = \frac{\delta}{R},\ \theta = \tan^{-1}\left(\frac{\delta}{R}\right) \quad (19)$$

Since the rotational displacement per one period of vibration is θ, the rotational speed Θ is expressed as follows, where f (Hz) is the driving frequency.

$$\Theta\ (\text{rad/s}) = f\,\theta \quad (20)$$

Although this analysis is performed on the horizontal plane, the mounting locations for components B and C are the same relative to the center G of the frame. Therefore, when the actuator is set on a vertical plane, the moments due to the gravity of components B and C cancel each other out. Consequently, for this actuator, in which the mass of the actuator is smaller than the attractive force due to the permanent magnet, the above analysis can also be applied to the vertical plane.

6. MEASUREMENT OF INPUT CURRENT TO VIBRATION COMPONENTS AND RESULTING AMPLITUDE

In the experiment, a steel plate 300 mm wide, 300 mm long, and 75 mm thick was used as the magnetic material. The resonance frequency f of the three vibration components was 104 Hz. Two two-channel signal generators were used to adjust the phase of the vibration in each component using a phase adjustment function. The sine waves generated by these signal generators were amplified by three amplifiers to drive each vibration component. The input current to the electromagnets in the components was measured using a power analyzer. When the vibration actuator was set on the iron plate, the attractive forces due to the main and secondary permanent magnets were P_1 = 2.4 N and P_2 = 0.59 N, respectively, with the rubber sheet. The coefficient of friction between the rubber sheet and the iron plate was μ = 0.84.

In the above static analysis, vibration amplitudes A_A, A_B and A_C are required. To evaluate the validity

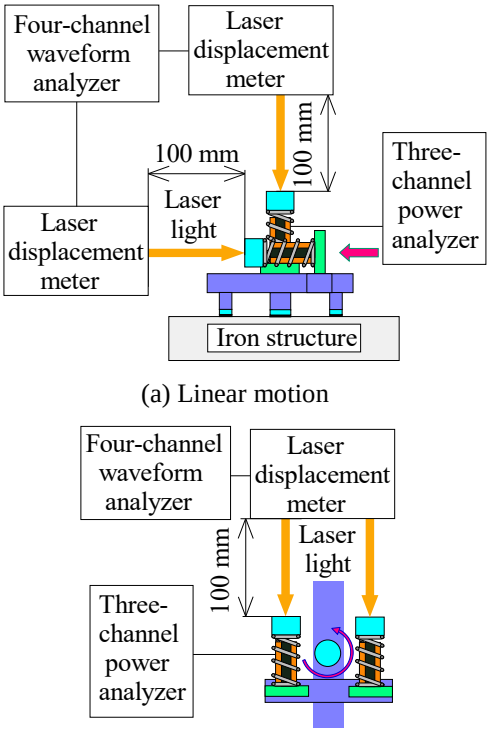

(a) Linear motion

(b) Rotational motion

Fig. 6. Experimental apparatus

of the theoretical analysis, the relationship between the input current to each component and the resulting vibration amplitude was measured for linear and rotational motions of the actuator. As shown in Fig. 6, a four-channel waveform analyzer, three laser displacement meters, and a three-channel power analyzer were used in the measurement.

For linear motion, a laser displacement meter was placed at the movement point of the actuator, as shown in Fig. 6(a). Vibration amplitudes A_A, B_A, and A_C were measured simultaneously using a waveform analyzer. Since the vibration components were prototyped to have identical dimensions, the vibration amplitudes of components B and C were equal. Using a power analyzer, the input currents to the vibration components were measured.

Similarly, the input current to each component and the resulting vibration amplitude during rotational motion were measured using the experimental apparatus shown in Fig. 6 (b). Linear and rotational motion measurements were made in the horizontal and vertical planes.

Fig. 7 shows the relationship between the input current to components B and C and the resulting vibration amplitude for linear and rotational motions. The plotted points show the average values for the cases of horizontal movement and vertical upward movement. The measurement results show almost no difference between the horizontal and vertical planes. The solid line was obtained using a least-

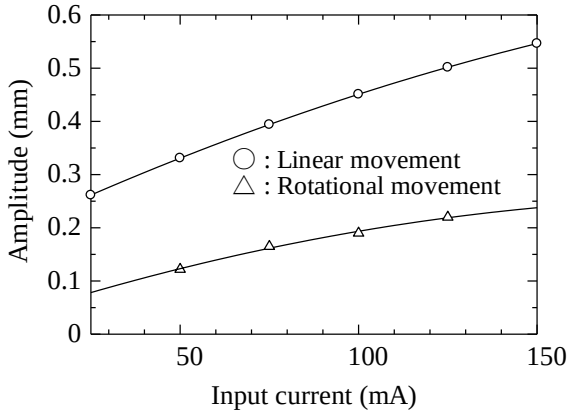

Fig. 7. Relationship between input current and resulting vibration amplitude

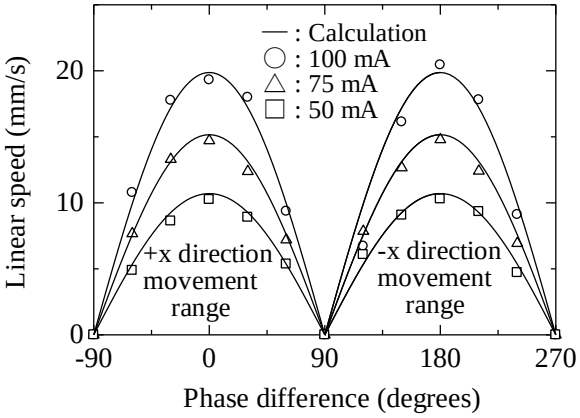

Fig. 8. Relationship between phase difference and linear speed

squares approximation of the plotted points using a quadratic equation. Based on the obtained measurement results, the relationship between the input current I (mA) to vibration component B (C) and the amplitude A_B (A_C) during linear and rotational motions was approximated as follows. For linear motion:

$$A_B\,(mm) = -4.9\times10^{-6}\times I^2 + 3.14\times10^{-3}\times I + 0.186 \quad \cdots\cdots (21)$$

For rotational motion:

$$A_B(mm) = -5.2\times10^{-6}\times I^2 + 2.19\times10^{-3}\times I + 0.027 \quad \cdots\cdots (22)$$

The approximation formulas are different for the same input current because the vibration modes for the two types of motion are different. In the future, the vibration amplitude of each vibration component will be calculated using a dynamic analysis of the vibration actuator.

Vibration amplitude A_A is 1.30 and 1.50 mm when a current of 50 and 75 mA is passed through component A, respectively. There was no difference between the horizontal and vertical planes.

7. CHARACTERISTICS OF LINEAR MOTION

First, components B and C were vibrated in phase and the linear motion characteristics of the actuator were measured.

Fig. 8 shows the relationship between the phase difference between component A and components B (and C) and the linear speed when the actuator is set in the horizontal plane for various input currents to components B and C. The input current to component A was 75 mA. The plotted points are the measurement results and the solid line was calculated using equations (10) and (21). When the phase difference between components A and B (and C) is 0 (in phase) and 180 degrees (out of phase), the linear speed of the actuator is maximized. In addition, since the linear speeds at 0 and 180 degrees are almost the same, the actuator can reciprocate at the same speed.

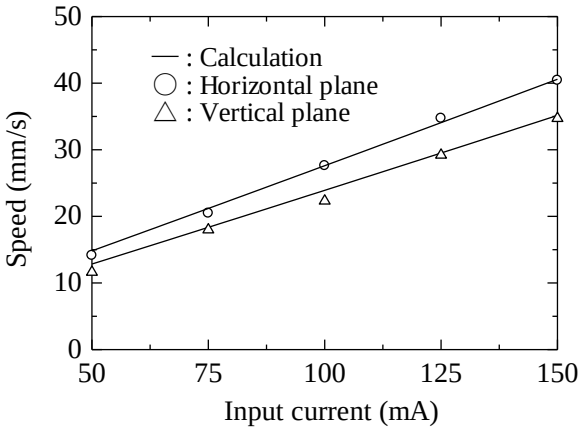

Fig. 9. Relationship between input current and linear speed

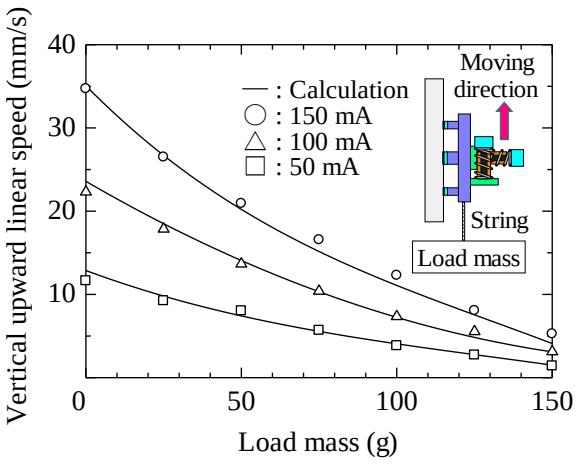

Fig. 10. Relationship between load mass and vertical upward linear speed

Fig. 9 shows the relationship between the input current to components B and C and the linear speed in the horizontal and vertical planes, with the input current to vibration component A fixed at 75 mA. From this figure, the measurement results and analysis results are in good agreement.

Fig. 10 shows the relationship between the mass loaded on the actuator and the vertical upward linear speed, with the input current to component A fixed at 75 mA and the input current to components B and C varied. The load mass was attached to the frame of the actuator using a string. In the figure, ○, △, and □ marks are the measurement results when the input current to component B (and C) was changed to 150, 100, and 50 mA, respectively. The solid line was calculated using equations (10) and (21) with β = 90 degrees. As can be seen, the vibration actuator can pull an additional mass of 150 g. Also, the plotted points are along the solid line.

8. CHARACTERISTICS OF ROTATIONAL MOTION

Components B and C were vibrated out of phase and the rotational motion of the actuator was investigated.

Fig. 11 shows the phase difference between component A and component B (C was always out of phase with B) and the rotational speed when the actuator was set in the horizontal plane, with the input current to components B and C set to 75 or 100 mA. The input current to component A was 50 mA. The plotted points are the measurement results and the solid line was calculated using equations (20) and (22). The rotational speeds of the actuators are almost equal when the phase difference between vibration components A and B is 0 degrees (in phase) and 180 degrees (out of phase). By controlling the phase of vibration in each component, the actuator can rotate clockwise and counterclockwise at the same rotational speed.

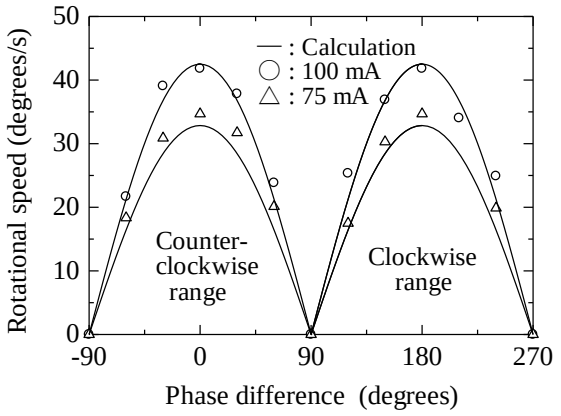

Fig. 11. Relationship between phase difference and rotational speed

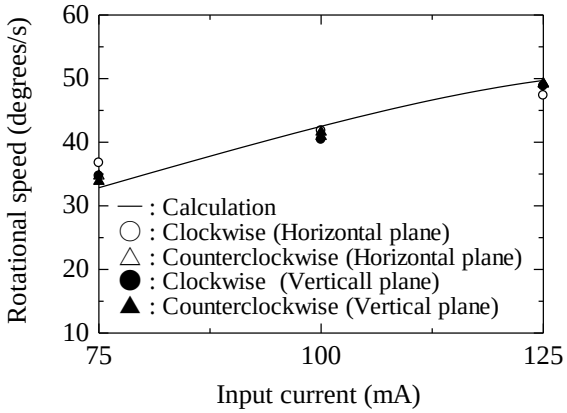

Fig. 12. Relationship between input current and rotational speed

Fig. 12 shows the relationship between the input current to components B and C and the rotational speed in the horizontal and vertical planes, with the input current to component A fixed at 50 mA. In the figure, ○ and ● (Δ and ▲) marks are the measurement results when rotating clockwise (counterclockwise) in the horizontal and vertical planes. The solid line was calculated using equations (20) and (22). As can be seen, the measurement and analysis results are in general agreement.

The results obtained in the machine test and the analysis results are mostly in agreement. This confirms that even if the parameters for the vibration actuator are varied, the linear and rotational characteristics of the actuator can be predicted by theoretical calculations.

9. CONCLUSIONS

A vibration actuator capable of movement in all directions by combining linear and rotational motions was proposed. It was shown that an actuator with orthogonally arranged vibration components can control linear and rotational reciprocating motions with the same characteristics by controlling the phase difference for vibrations. A static analysis of linear and rotational motion of the actuator using the energy method was performed, and the results obtained were compared and discussed with the measurement results from actual machine tests. It was shown that the measured and calculated values were in relatively good agreement.

By measuring the relationship between the input current to the electromagnet and the resulting vibration amplitude in the mounted vibration component, a design index for the actuator can be predicted. In this paper, the principle of operation of a compact, lightweight, and controllable actuator was newly established. In the future, by mounting a camera on the actuator, it becomes possible to inspect the appearance of the iron bridge.

This paper demonstrates the potential for realizing social infrastructure improvement in large steel structures such as bridges.

10. ACKNOWLEDGMENTS

The authors would like to thank the International Journal of GEOMATE for its prompt and accurate peer review and helpful suggestions in the publication of this paper. Furthermore, this work was supported by JSPS KAKENHI Grant Number JP23K03648.

11. REFERENCES

[1] Suzuki M., and Hirose S., Proposal of Swarm Type Wall Climbing Robot System Anchor Climber and Development of Adhering Mobile Units, The Robotics Society of japan, Vol. 28, No. 5, 2010, pp. 614-623.

[2] Hagiwara T., Yamamura Y., Namima Y., Ogami J., and Pengfei L., Production of Crawler Robot with Sub Crawler and Verification of Traversing Ability, 2021 Second International Symposium on Instrumentation, Control, Artificial Intelligence, and Robotics (ICA-SYMP), 2021, pp. 1 - 4.

[3] Kumar S., and Arora M., Design and Application of Crawler Robot, 6th National Conference on Advancements in Simulation and Experimental Techniques in Mechanical Engineering (NCASEme), 2019, pp. 90 - 94.

[4] Shen W., Gu J., and Shen Y., Permanent motion System Design for the Wall-Climbing Robot, in Proc., IEEE International Conference on Mechatronics & Automation, 2011, pp. 2078-2083.

[5] Yaguchi H., and Itoh Y., Vibration Actuator System for Internal Inspection of Large Complex Iron Structures, International Journal of GEOMATE, Vol. 22, No. 89, 2022, pp. 9 - 15.

[6] Yaguchi H., and Itoh Y., Vibration Actuator System with Small-Scale Size Capable of Visual Inspection of Large Complex Iron Structures, Applied Sciences, Vol. 11, No. 16, 2021, pp. 1 - 16.

[7] Hanimura N., Okamoto Y., Toga S., and Nakamura S., A Study on the Design Method of Magnetic Wheel for Low Power Consumption of Magnetic Levitation Robots, 2021 International Conference on Advanced Mechatronic Systems, 2021, pp. 1 - 5.

[8] Qin W., and Bird J., Electrodynamic Wheel Magnetic Rolling Resistance, IEEE Transactions on Magnnetics, vol. 53, No. 8, 2017, DOI:10.1109/TMAG.2017.2693962.

[9] Khirade N., Sanghi R., and Tidke D., Magnetic Wall Climbing Devices - A Review, in Proc., International Conference on Advances in Engineering & Technology, 2014, pp.55-59.

[10] Rushood M., Rahbar F., Shokri S., Selim S., and Dweiri F., Accelerating Use of Drones and Robotics in Post-Pandemic Project Supply Chain, Drones, 2023, Vol. 7, No. 5, pp. 1 - 9.

[11] Mahamud N., Muhammad G., Shahriar H., Khan H., Sharmin S., and Lisa N., ALW drone : A New Design and Efficient Approach, in Proc., IEEE 19th International Conference on Computer and Information Technology, 2017, pp. 474-479.

[12] Morita M., Kinjo H., Sato S., Sulyon T., and Anezaki T., Autonomous Flight Drone for Infrastructure (transmission line) Inspection, in Proc., IEEE International Conference on Intelligent Informatics and Biomedical Sciences (ICIIBMS), 2017, pp. 198-201.

[13] Jae S., Donghoon K., Heon J., and Hyun M., Micro Aerial Vehicle Type Wall-climbing Robot Mechanism, in Proc., IEEE RO-MAN International Symposium on Robot and Human Interactive Communication, 2013, pp. 722-725.

[14] Furukawa A., and Jiang M., Estimating Natural Vibration Characteristics of Bridge Cables Based on N4SID Subspace Method, International Journal of GEOMATE, Vol. 26, Issue 113, 2024, pp. 98-106.

[15] Tuleyev A., Omarov Z., Abakanov T., Lapin T., and Tuleyev T., Vibration Test of A High-Rise Monolithic Building, International Journal of GEOMATE, Vol. 25, Issue 109, 2023, pp.149-156.

[16] Furukawa A., Yamada S., and Kobayashi R., Tension Estimation Methods for NIELSEN-LOHSE Bridges using Out-of-Plane and In-Plane Natural Frequencies, International Journal of GEOMATE, Vol.23, Issue 97, 2022, pp.1-11.

[17] Urakawa A., Sasaki T., and Cho H., Dynamic Properties of Post-Buckled Shape Memory Alloy and its Application to a Base Isolator for Vertical Vibration, International Journal of GEOMATE, Vol.20, Issue 82, 2021, pp.101-108.

[18] Chen J., Jiang J., Wang K., and Zhang F., Optimal Placement of Actuators for Active Vibration Control Using EER and Genetic Algorithm, IEEE 10th International Conference on Mechanical and Aerospace Engineering (ICMAE), 2019, pp. 459- 453.

[19] Li J., Xue Y., Li F., and Narita Y., Active Vibration Control of Functionally Graded Piezoelectric Material Plate, Composite Structures, Vol. 207, No. 1, 2019, pp. 509-518.

[20] Yaguchi H., and Yamori S., Magnetic Actuator Capable of In-Plane Movement by Phase Control of Vibration Components, IEEE Transactions on Magnetics, Vol. 58, No. 8, 2022, pp. 1 - 6

[21] Yaguchi H., A New Type of Electromagnetically Propelled Vibration Actuator for Appearance Inspection of Iron Structure, International Journal of GEOMATE, Vol. 20, No. 77, 2021, pp. 69 - 76.

[22] Yaguchi H., Watanabe T., and Mishina T., A New Type of Magnetic Pump with Coupled Mechanical Vibration and Electromagnetic Force, International Journal of GEOMATE, Vol. 23, No. 99, 2022, pp. 119 - 125.

[23] Aoki H., and Kitani S., Industrial mechanics (Four edition), Vol. 9, 2021, pp. 120 - 122.